J. Mech. Phys. Solids Vol. 37, No. 5, pp. 567–582, 1989.
Printed in Great Britain.

0022–5096/89 $3.00+0.00

CUSP CATASTROPHE INTERPRETATION OF FRACTURE INSTABILITY

ALBERTO CARPINTERI

Department of Structural Engineering, Politecnico di Torino, 10129 Torino, Italy

(*Received* 15 *February* 1988; *in revised form* 26 *July* 1988)

ABSTRACT

A COHESIVE crack model is applied to analyse slow crack growth in elastic-softening materials. The shape of the structural load–displacement response is changed substantially by varying the size-scale while keeping the geometrical shape of the structure unchanged. The softening branch becomes steeper when the size-scale increases. A critical size-scale exists for which the softening slope is infinite. In such a case the load carrying capacity drastically decreases for relatively small displacement increments. Then, for size-scales larger than the critical one, the softening slope becomes positive and part of the load–displacement path becomes virtual if the loading process is displacement-controlled. In such a case, the loading capacity will present a discontinuity with a negative jump. The size-scale transition from ductile to brittle behaviour is governed by a nondimensional brittleness number s_E which is a function of material properties and structure size-scale. A truly brittle failure occurs only with relatively low fracture toughnesses $\mathscr{G}_{IC}$, high tensile strengths σ_u, and/or large structure size-scales b, i.e. when $s_E = \mathscr{G}_{IC}/\sigma_u b \to 0$.

On the other hand, if the loading process is controlled by a monotonically increasing function of time (e.g. the crack mouth opening displacement), the snap-back instability in the load–displacement curve can be captured experimentally. When the post-peak behaviour is kept under control up to the complete structure separation, the area delimited by the load–displacement curve and the displacement-axis represents the product of $\mathscr{G}_{IC}$ and the initial ligament area.

Finally, it is verified that, for $s_E \to 0$, the maximum load for catastrophic failure is provided by the simple LEFM condition: $K_I = K_{IC} = \sqrt{\mathscr{G}_{IC} E}$ (plane stress), and that there is no slow crack growth prior to instability.

1. INTRODUCTION

IT IS OBSERVED experimentally that, in some cases, the plastic zone at the crack tip develops as a localized strain field colinear to the initial crack line. In other cases, the crack tip plastic zone is diffused in a wider band or even presents a butterfly-shape, when the material is particularly ductile. The *cohesive crack model* considered in this work is a representative model only when the plastic zone is confined to a very narrow band. It consists of an ideal crack, including in its length also the real plastic zone, with restraining forces which close the crack tip faces and simulate the effects of plasticity. In fact, such forces are usually non-increasing functions of the distance between the crack surfaces. Softening cohesive relationships between force and crack opening reveal themselves to be very accurate in describing crack behaviour and strain localization in cementitious and polymeric (fibre-reinforced) composites.

The cohesive crack model was originally proposed by BARENBLATT (1959), who considered the interatomic restraining forces near the crack tip confined to an interaction zone of constant size. The shape of the terminal crack region was supposed to be fixed even if translating, while the stress at the end of the crack , due to external load and cohesive force distribution, was assumed to be finite.

A similar analysis was independently conducted by DUGDALE (1960) to study the extent of plastic yielding in steel sheets (of infinite size) containing an initial crack. The cohesive model was reconsidered by BILBY, COTTRELL and SWINDEN (1963) and the distribution of plastic strain in the yielded region was represented by an inverted pile-up of dislocations. A comparison of the crack growth criteria of GRIFFITH (1921) and BARENBLATT (1959) was provided by WILLIS (1967), who proved the coincidence of the modulus of cohesion with the critical stress-intensity factor. Then, RICE (1968) observed that the critical value of the J-integral is equal to the area under the diagram of stress vs crack opening displacement.

In the last few years, the *cohesive crack model* was reproposed, with some modifications, by WNUK (1974)—the Final Stretch Model—and by HILLERBORG, MODEER and PETERSSON (1976)—the Fictitious Crack Model. The latter was applied mostly to concrete-like materials and numerically implemented in a finite element program. Lastly, FOOTE, MAI and COTTERELL (1986) developed a theoretical model able to show that the K_R curve is almost unique and independent of specimen geometry and initial crack length.

In the present paper the *cohesive crack model* is applied to analyse stable vs unstable crack propagation in elastic-softening materials. The shape of the structural load–displacement response changes substantially by varying the size-scale while keeping the geometrical shape of the structure unchanged. For size-scales larger than a threshold value, a snap-back instability appears, when the plastic zone is still absent and the slow crack growth has not yet occurred. Asymptotically, the snap-back load may be provided by the simple LEFM condition: $K_I = K_{IC}$ (CARPINTERI, 1985).

The snap-back load–displacement branch may be captured experimentally if the loading process is controlled by a monotonically increasing function of time, such as the crack mouth opening displacement.

The size-scale transition from ductile to brittle behaviour is governed by a dimensionless brittleness number s_E, which is a function of material properties and structure size-scale. A truly brittle failure occurs only with relatively low fracture toughnesses, $\mathcal{G}_{IC}$, high tensile strengths σ_u, and/or large structure size-scales b, i.e. when $s_E = \mathcal{G}_{IC}/\sigma_u b \to 0$.

A Dimensional Analysis application to fracture mechanics is presented. It is shown that, due to the different physical dimensions of strength, $[F]\ [L]^{-2}$, and toughness, $[F]\ [L]^{-1}$, scale effects are always present in the experimental testing of common engineering materials (CARPINTERI, 1981, 1982). The virtual propagation of a brittle fracture is also considered. Such an approach is analogous to that of BERRY (1960) and demonstrates that large cracks are more stable than small cracks. The same trend was recently confirmed experimentally by BIOLZI, CANGIANO, TOGNON and CARPINTERI (1987).

An algorithm to describe cohesive crack propagation is presented in Section 2, whereas the size-scale transition from ductile to brittle failure is dealt with in Section

3. The brittleness-ratio of ultimate elastic energy to energy dissipated in the fracture process is introduced in Section 4. This ratio tends to infinity, for the size tending to infinity, when the element is initially uncracked. On the other hand, it tends to a finite quantity when there is an initial crack. In the latter case, the snap-back load–displacement branch is always distinct from the elastic one.

2. Cohesive Crack Propagation

The cohesive crack model is based on the following assumptions.

(1) The cohesive fracture zone (plastic or process zone) begins to develop when the maximum principal stress achieves the ultimate tensile strength σ_u (Fig. 1a).

(2) The material in the process zone is partially damaged but still able to transfer stress. Such a stress can be considered as linearly dependent on the crack opening displacement w (Fig. 1b).

The energy necessary to produce a unit crack surface is given by the area under the σ–w diagram in Fig. 1b:

$$\mathcal{G}_{IC} = \int_0^{w_c} \sigma \, dw = \tfrac{1}{2}\sigma_u w_c.$$

The *real crack tip* is defined as the point where the distance between the crack surfaces is equal to the critical value of crack opening displacement w_c and the normal stress vanishes (Fig. 2a). On the other hand, the *fictitious crack tip* is defined as the point where the normal stress attains the maximum value σ_u and the crack opening vanishes (Fig. 2a).

A three point bending slab of elastic-softening material is considered (Fig. 3). The displacement discontinuity on the centre line may be expressed as follows:

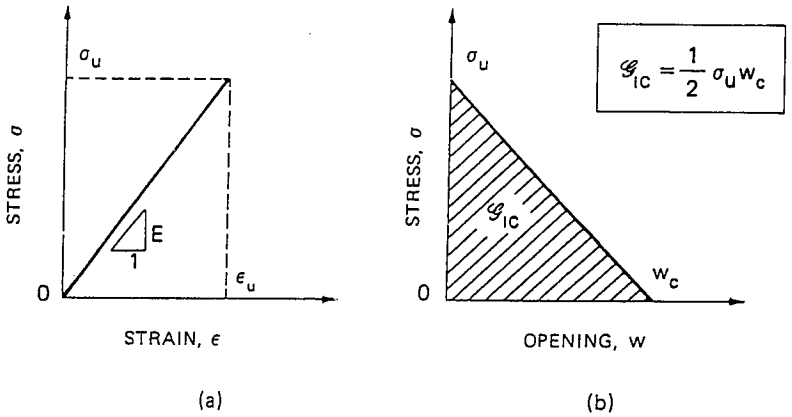

FIG. 1. Stress–strain (a) and stress–crack opening displacement (b) constitutive laws.

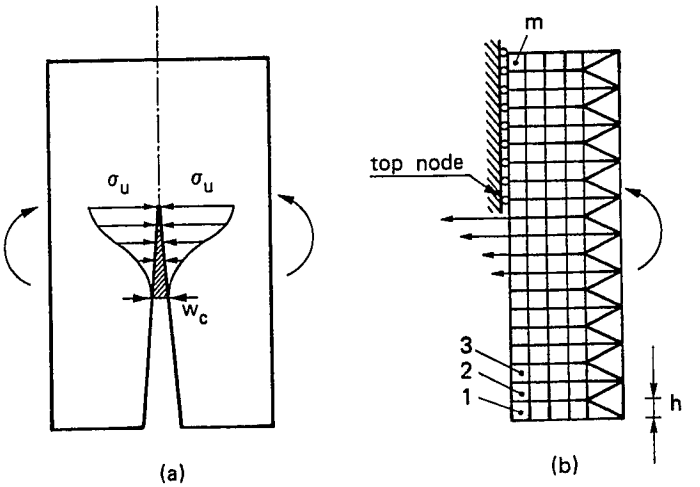

FIG. 2. Stress distribution across the cohesive zone (a) and equivalent nodal forces in the finite element mesh (b).

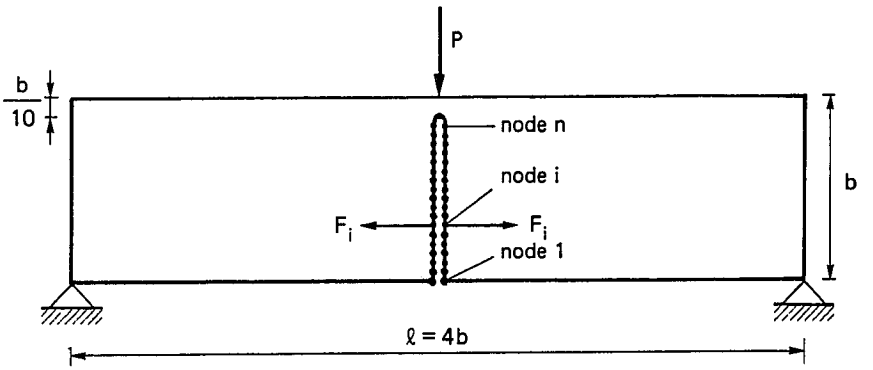

FIG. 3. Finite element nodes along the potential fracture line.

$$w(x) = \int_0^b K(x,y)\sigma(y)\,dy + C(x)P + \Gamma(x) \quad \text{for} \quad 0 \leqslant x < b, \tag{1}$$

where K and C are the influence functions of cohesive forces and external load respectively, and Γ is the crack opening due to the specimen weight. If a stress-free crack of length a has developed with a cohesive zone of length Δa the following additional conditions are to be taken into account:

$$\sigma(y) = 0, \quad \text{for} \quad 0 \leqslant y \leqslant a, \tag{2a}$$

$$\sigma(y) = \sigma_u\left[1 - \frac{w(y)}{w_c}\right], \quad \text{for} \quad a \leqslant y \leqslant (a+\Delta a), \tag{2b}$$

$$w(x) = 0, \quad \text{for} \quad (a+\Delta a) \leqslant x < b. \tag{2c}$$

Equations (1) and (2) can be rearranged as follows:

$$w(x) = \int_a^{a+\Delta a} K(x,y)\left[1-\frac{w(y)}{w_c}\right]\sigma_u \,\mathrm{d}y + \int_{a+\Delta a}^{b} K(x,y)\sigma(y)\,\mathrm{d}y + C(x)P + \Gamma(x), \quad \text{for} \quad 0 \leqslant x \leqslant (a+\Delta a), \tag{3a}$$

$$w(x) = 0, \quad \text{for} \quad (a+\Delta a) \leqslant x < b. \tag{3b}$$

The function $\sigma(y)$ depends on the distribution $w(x)$ and on the external load P. Therefore, for each value of P, (3a) represents an integral equation for the unknown function w. On the other hand, the beam deflection is given by

$$\delta = \int_0^b C(y)\sigma(y)\,\mathrm{d}y + D_p P + D_\gamma, \tag{4}$$

where D_p is the deflection for $P = 1$ and D_γ is the deflection due to the specimen weight.

A numerical procedure is implemented to simulate a loading process where the parameter incremented step by step is the fictitious crack depth. Real (or stress-free) crack depth, external load and deflection are obtained at each step after an iterative computation. The closing stresses acting on the crack surfaces (Fig. 2a) are replaced by nodal forces (Fig. 2b). The intensity of these forces depends on the opening of the fictitious crack w, according to the σ–w constitutive law of the material (Fig. 1b). When the tensile strength σ_u is achieved at the fictitious crack tip (Fig. 2b), the top node is opened and a cohesive force starts acting across the crack, while the fictitious crack tip moves to the next node.

With reference to the three point bending test (TPBT) geometry in Fig. 3, the nodes are distributed along the potential fracture line. The coefficients of influence in terms of node openings and deflection are computed by a finite element analysis where the fictitious structure in Fig. 3 is subjected to $(n+1)$ different loading conditions. Consider the TPBT in Fig. 4a with the initial crack tip in the node k. The crack opening displacements at the n fracture nodes may be expressed as follows:

$$\mathbf{w} = \mathbf{K}\mathbf{F} + \mathbf{C}P + \boldsymbol{\Gamma}, \tag{5}$$

where

$\mathbf{w}$ = vector of the crack opening displacements,
$\mathbf{K}$ = matrix of the coefficients of influence (nodal forces),
$\mathbf{F}$ = vector of the nodal forces,
$\mathbf{C}$ = vector of the coefficients of influence (external load),
P = external load,
$\boldsymbol{\Gamma}$ = vector of the crack opening displacements due to the specimen weight.

On the other hand, the initial crack is stress-free and therefore

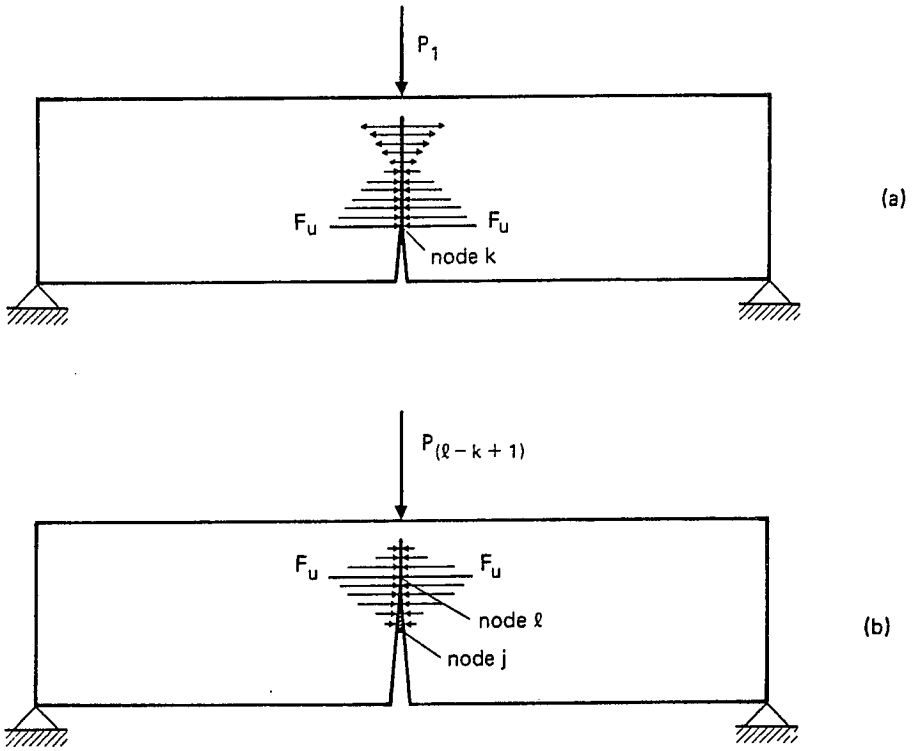

FIG. 4. Cohesive crack configurations at the first (a) and $(l-k+1)$th (b) crack growth increment.

$$F_i = 0, \quad \text{for} \quad i = 1,2,\ldots,(k-1), \tag{6a}$$

while at the ligament there is no displacement discontinuity:

$$w_i = 0, \quad \text{for} \quad i = k,(k+1),\ldots,n. \tag{6b}$$

Equations (5) and (6) constitute a linear algebraic system of $2n$ equations and $2n$ unknowns, i.e. the elements of vectors $\mathbf{w}$ and $\mathbf{F}$. If load P and vector $\mathbf{F}$ are known, it is possible to compute the beam deflection δ:

$$\delta = \mathbf{C}^T\mathbf{F} + D_P P + D_\gamma. \tag{7}$$

After the first step, a cohesive zone forms in front of the real crack tip (Fig. 4b), say between nodes j and l. Then Eqs (6) are replaced by

$$F_i = 0, \quad \text{for} \quad i = 1,2,\ldots,(j-1), \tag{8a}$$

$$F_i = F_u\left(1 - \frac{w_i}{w_c}\right), \quad \text{for} \quad i = j,(j+1),\ldots,l, \tag{8b}$$

$$w_i = 0, \quad \text{for} \quad i = l,(l+1),\ldots,n, \tag{8c}$$

where F_u is the ultimate strength nodal force (Fig. 2b):

$$F_u = b\sigma_u/m. \tag{9}$$

Equations (5) and (8) constitute a linear algebraic system of $(2n+1)$ equations and $(2n+1)$ unknowns, i.e. the elements of vectors **w** and **F** and the external load P.

At the first step, the cohesive zone is missing ($l = j = k$) and the load P_1 producing the ultimate strength nodal force F_u at the initial crack tip (node k) is computed. Such a value P_1, together with the related deflection δ computed through (7), gives the first point of the P–δ curve. At the second step, the cohesive zone is between the nodes k and $(k+1)$, and the load P_2 producing the force F_u at the second fictitious crack tip (node $k+1$) is computed. Equation (7) then provides the deflection δ_2. At the third step, the fictitious crack tip is in the node $(k+2)$, and so on. The present numerical program simulates a loading process where the controlling parameter is the fictitious crack depth. On the other hand, real (or stress-free) crack depth, external load and deflection are obtained at each step after an iterative procedure.

The program stops with the untying of the node n and, consequently, with the determination of the last couple of values F_n and δ_n. In this way, the complete load–deflection curve is automatically plotted by the computer.

3. Size-scale Transition from Ductile to Catastrophic Failure

Let us consider a cracked beam in flexure with the span ℓ, equal to four times the beam depth b (Fig. 3). Such sizes will be scaled with geometrical similitude, whereas the beam thickness will be kept constant, $t = 10$ cm. The initial crack depth a_0/b, will range between 0.0 (initially uncracked beam) and 0.5. The mechanical properties are those typical of a concrete-like material:

Young's modulus $E = 400\,000$ kg cm^{-2},
ultimate tensile strength $\sigma_u = 40$ kg cm^{-2},
critical crack opening displacement $w_c = 0.005$ cm.

The area under the σ vs w curve in Fig. 1b is the strain energy release rate $\mathcal{G}_{IC} = \frac{1}{2}\sigma_u w_c = 0.1$ kg cm^{-1}.

For the size-scale parameter $b = 10$ cm, the load–deflection curves are reported in Fig. 5a by varying the initial crack depth a_0/b. For deep cracks, stiffness and loading capacity decrease, whereas ductility increases. The slope of the softening branch achieves its maximum when the beam is initially uncracked.

The load–deflection curves in Fig. 5b relate to the case $b = 20$ cm. The general trend by varying the geometrical ratio a_0/b is the same as in Fig. 5a. In this case, however, the maximum softening slope for $a_0/b = 0$ is nearly infinite and a drop in the load carrying capacity is predicted when $\delta \simeq 12 \times 10^{-3}$ cm.

The case $b = 40$ cm is described in Fig. 5c. For $a_0/b \lesssim 0.20$, the softening slope presents even positive values with snap-back of the P–δ curve. If the loading process is deflection-controlled, the load will present a discontinuity with a negative jump. Substantially, this is the case of a cusp catastrophe.

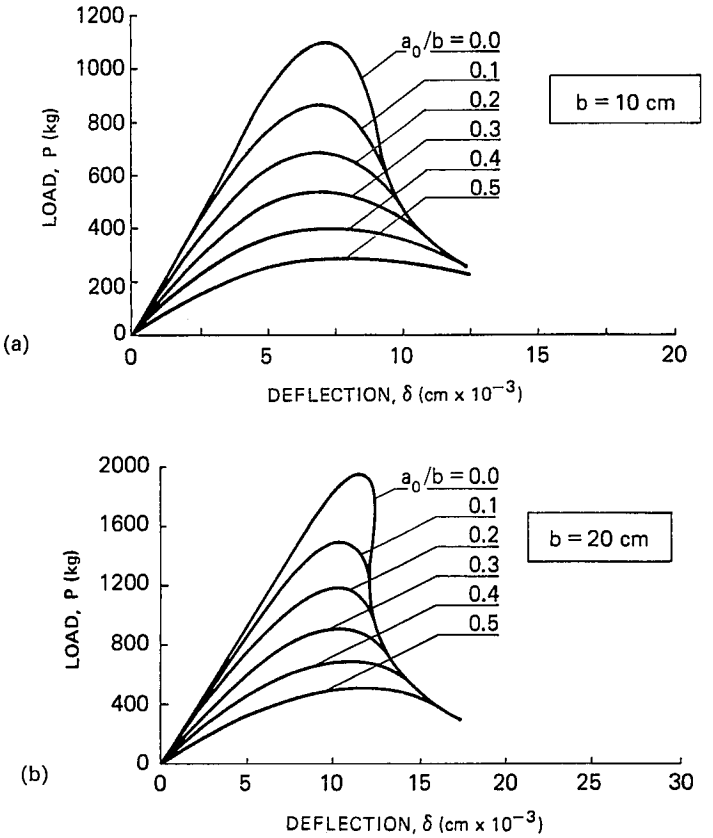

FIG. 5. Load–deflection curves obtained by varying the initial crack depth a_0/b. (a) $b = 10$ cm; (b) $b = 20$ cm; (c) $b = 40$ cm; (d) $b = 80$ cm.

The case $b = 80$ cm is eventually contemplated in Fig. 5d. The cusp catastrophe occurs for $a_0 b \lesssim 0.25$. That is, when the size-scale increases, the initial crack depth interval of the cusp catastrophe spreads.

The opposite trends of brittleness increase by increasing size-scale and/or decreasing initial crack depth, are shown schematically in Fig. 6. The gradual transition from simple fold catastrophe to bifurcation or cusp catastrophe generates an equilibrium surface (or catastrophe manifold).

Such theoretical results were confirmed by BIOLZI *et al.* (1987) through an experimental investigation on high strength concrete beams. The mechanical response of the specimens with deep cracks appeared stable (Fig. 7a). Both load–deflection and load–CMOD curves showed the same shape with a softening branch of negative slope. By decreasing the relative crack depth such a branch becomes steeper with an increase in the brittleness of the system. At the same time, obviously, loading capacity and stiffness increase.

The specimens with shallow cracks (Fig. 7b) on the contrary, presented a very unstable behaviour. Whereas the load–CMOD curves have a softening tail with

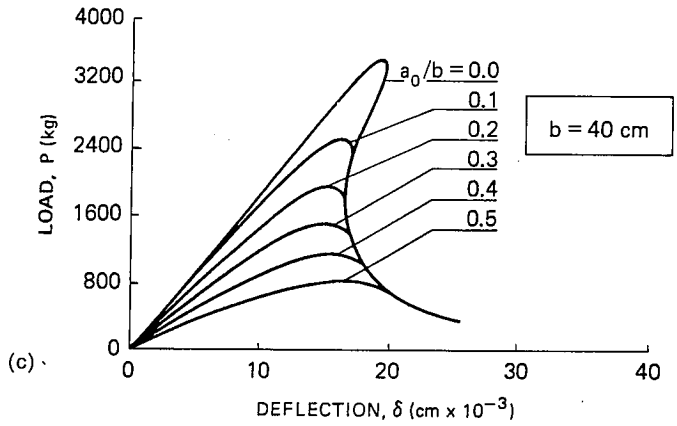

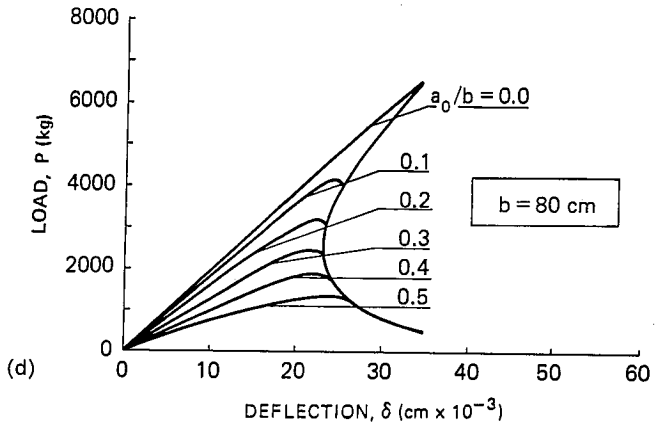

FIG. 5.—*continued.*

negative slope, the load–deflection curves are characterized by a snap-back softening instability with a softening branch of partial positive slope. More precisely, the case $a_0 = 30$ mm shows an almost vertical drop in the loading capacity when the maximum load is achieved. This experimental finding confirms the theoretical results in Fig. 5. In fact, the relative crack depth $a_0/b = 0.3$ is the critical condition between stability and instability for deflection-controlled loading processes. If the loading process had been deflection-controlled, then, once the bifurcation point of the loading path had been reached, the load would have presented a negative jump down to the lower softening branch with a negative slope. Therefore, it is evident that, although the process is unstable in nature, it can develop in a stable manner if CMOD-controlled.

All the diagrams in Fig. 7 converge towards the same asymptotic tail, the limit situation being independent of the initial crack length.

The previous theoretical and experimental analyses emphasize that the (brittle or ductile) structural behaviour is connected with a geometrical feature, as is the case of

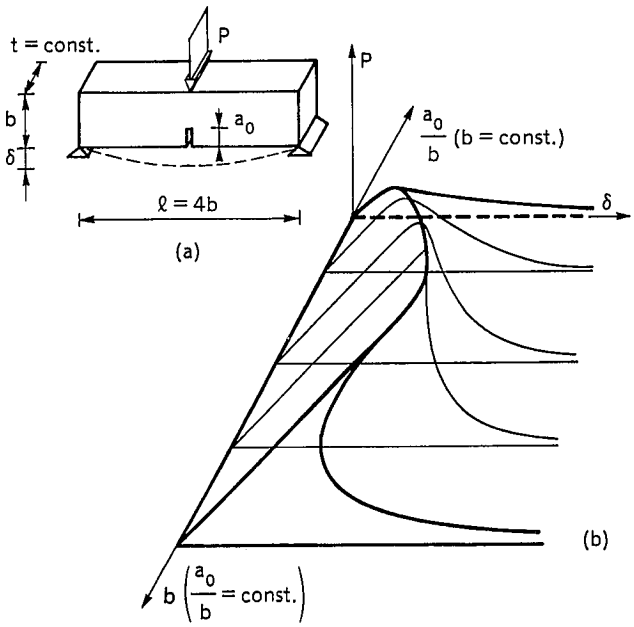

FIG. 6. Three point bending specimen (a) and catastrophe manifold (b).

the crack depth. More generally, all the geometrical features of the specimen influence the global brittleness (or ductility), and particularly slenderness and size-scale.

The maximum loading capacity $P^{(1)}_{max}$ according to the cohesive crack model is obtained from the P–δ diagrams in Fig. 5. On the other hand, the maximum load $P^{(2)}_{max}$ according to LEFM can be derived from the ASTM formula, with the critical value of stress-intensity factor K_{IC} computed according to the well-known relationship:

$$K_{IC} = \sqrt{\mathscr{G}_{IC} E}. \tag{10}$$

The values of the ratio $P^{(1)}_{max}/P^{(2)}_{max}$ are reported as functions of the dimensionless size, $b\sigma_u/\mathscr{G}_{IC}$, or equivalently, of the energy brittleness number, $s_E = \mathscr{G}_{IC}/\sigma_u b$ in Fig. 8. The ratio $P^{(1)}_{max}/P^{(2)}_{max}$ may also be regarded as the ratio of the fictitious fracture toughness (given by the non-linear maximum load) to the true fracture toughness (considered as a material constant).

It is evident that, for low s_E values, the results of the cohesive crack model tend to those of LEFM:

$$\lim_{s_E \to 0} P^{(1)}_{max} = P^{(2)}_{max} \tag{11}$$

and, therefore, the maximum loading capacity can be predicted applying the simple condition $K_I = K_{IC}$ (CARPINTERI, 1985).

The fictitious crack depth at the maximum load is plotted as a function of the inverse of brittleness number s_E in Fig. 9. The brittleness increase for $s_E \to 0$ is evident

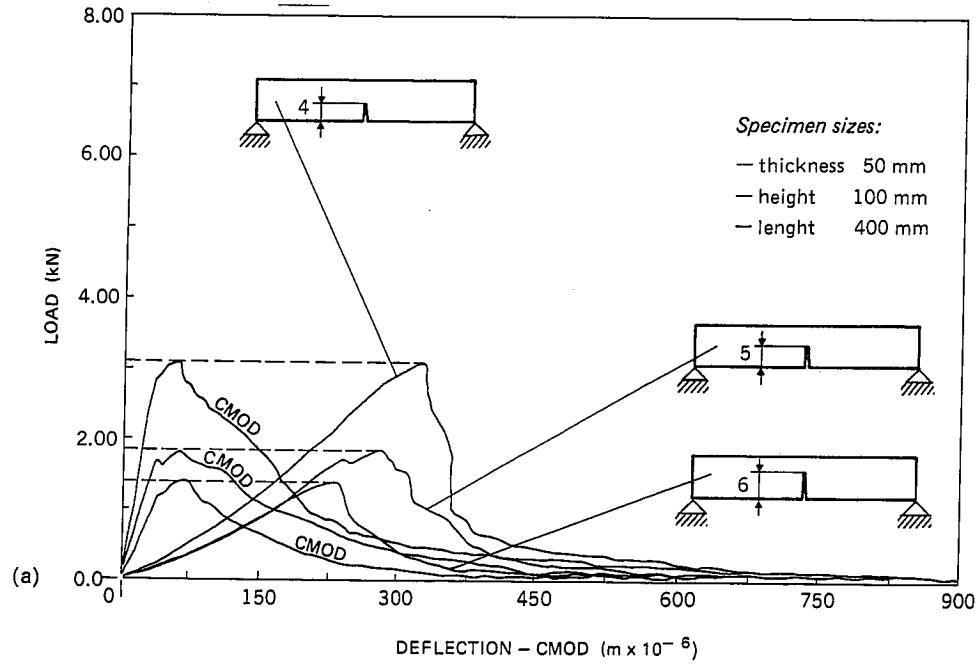

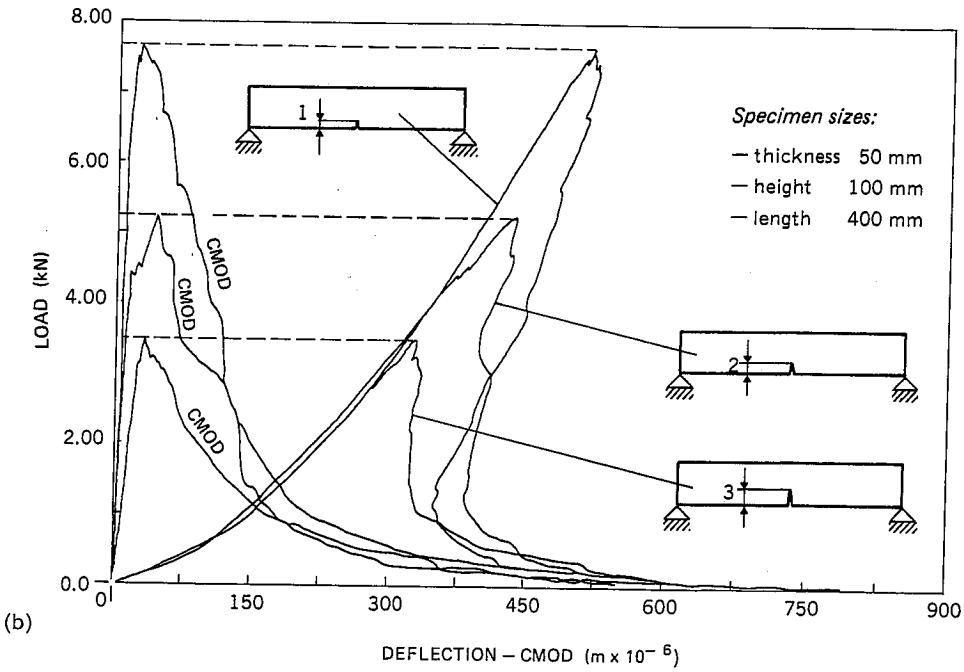

FIG. 7. (a) Experimental load–deflection and load–CMOD diagrams ($a_0/b = 0.4, 0.5, 0.6$), after BIOLZI *et al.* (1987); (b) experimental load–deflection and load–CMOD diagrams ($a_0/b = 0.1, 0.2, 0.3$), after BIOLZI *et al.* (1987).

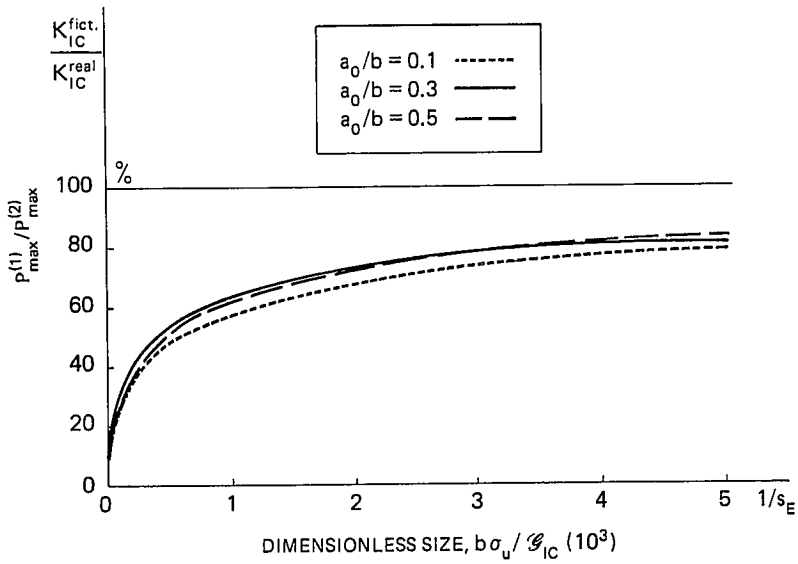

FIG. 8. Size-scale transition towards LEFM.

also from these diagrams, the process zone at $dP/d\delta = 0$ tending to disappear, whereas it tends to cover the whole ligament for $s_E \to \infty$ (ductile collapse). The real (or stress-free) crack depth at the maximum load is nearly coincident with the initial crack depth for each value of s_E. This means that the slow crack growth does not start before the softening stage. Therefore, neither the slow crack growth occurs nor the cohesive zone develops before the peak, when $s_E \to 0$.†

Recalling once again Figs 8 and 9, it is possible to state that, the smaller the brittleness number s_E is, i.e. the lower the fracture toughness $\mathcal{G}_{IC}$, the larger the size-scale b and/or the higher the ultimate tensile strength σ_u, the more accurate the cusp catastrophe is in reproducing the classical LEFM instability.

4. FRACTURE ENERGY DISSIPATION AND BRITTLENESS LIMIT FOR INFINITE SIZE-SCALE

If the loading process is controlled by a monotonically increasing function of time, like, for instance, the crack mouth opening displacement, the snap-back behaviour in the load–displacement curve can be captured experimentally. When the post peak behaviour is kept under control up to the complete structure separation, the area delimited by the load–displacement curve and displacement-axis represents the product of strain energy release rate $\mathcal{G}_{IC}$, with the initial ligament area $(b-a_0)t$, (Fig. 10).

†Slow crack growth and cohesive zone may develop only if both load and displacement are decreased, following the virtual branch with positive slope. On the other hand, with normal softening (i.e. only negative slope in the P–δ curve after the peak) only the load must be decreased to control the fracture process.

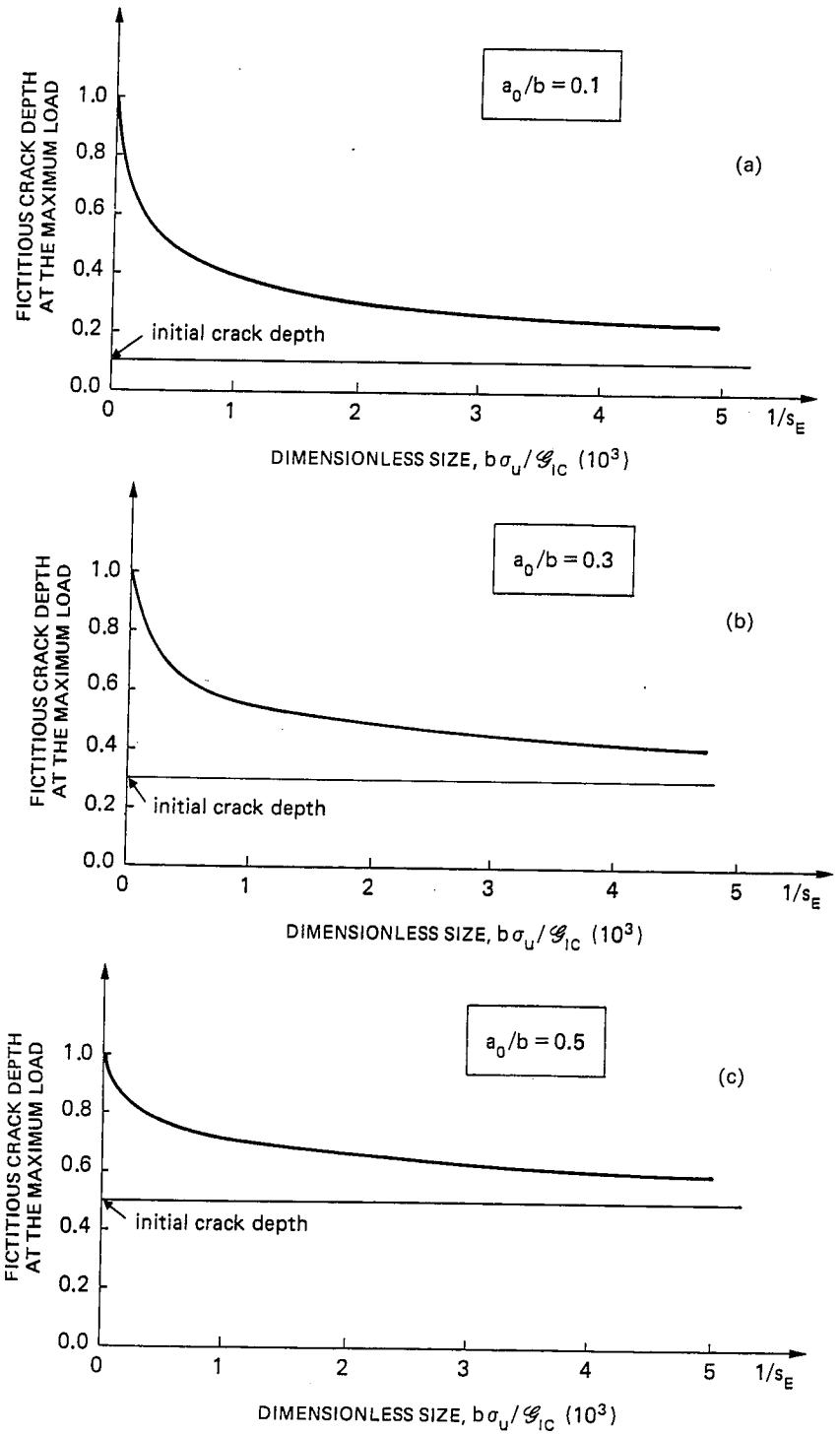

FIG. 9. Fictitious crack depth at the maximum load as a function of dimensionless size. (a) $a_0/b = 0.1$; (b) $a_0/b = 0.3$; (c) $a_0/b = 0.5$.

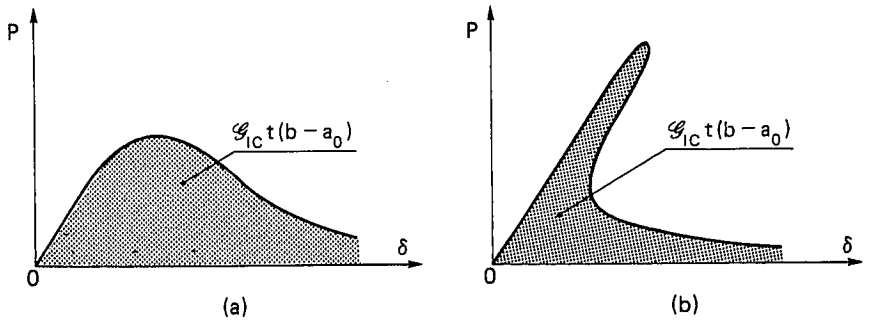

FIG. 10. Energy dissipated in the fracturing process. Ductile (a) and brittle (b) behaviour.

The area under the curve $a_0/b = 0.0$ is thus twice that under the curve $a_0/b = 0.5$ in Fig. 5a, as well as the half of that under the curve $a_o/b = 0.0$ in Fig. 5b, etc. This simple result is due to the assumption that energy dissipation occurs only on the fracture surface, while in reality energy is also dissipated in a damage volume around the crack tip. When the brittleness number $s_E \to 0$, $P^{(1)}_{max} \simeq P^{(2)}_{max}$ and (10) provides:

$$\mathcal{G}_{IC} = P^2_{max} \frac{(\ell/b)^2 f^2(a_0/b)}{bt^2 E} \tag{12}$$

being:

$$K_{IC} = \frac{P_{max}\ell}{tb^{3/2}} f\left(\frac{a_0}{b}\right), \tag{13a}$$

$$f\left(\frac{a_0}{b}\right) = 2.9\left(\frac{a_0}{b}\right)^{1/2} - 4.6\left(\frac{a_0}{b}\right)^{3/2} + 21.8\left(\frac{a_0}{b}\right)^{5/2} - 37.6\left(\frac{a_0}{b}\right)^{7/2} + 38.7\left(\frac{a_0}{b}\right)^{9/2}. \tag{13b}$$

In a three point bending specimen of linear elastic material the deflection is given by the contribution of a distributed and a concentrated compliance respectively (TADA, PARIS and IRWIN, 1963):

$$\delta = \frac{P}{Et}\left[\frac{1}{4}\left(\frac{\ell}{b}\right)^3 + \frac{3}{2}\left(\frac{\ell}{b}\right)^2 g\left(\frac{a_0}{b}\right)\right], \tag{14}$$

where $g(a_0/b)$ is given by:

$$g\left(\frac{a_0}{b}\right) = \left(\frac{a_o/b}{1-\frac{a_0}{b}}\right)^2 \left\{5.58 - 19.57\left(\frac{a_0}{b}\right) + 36.82\left(\frac{a_0}{b}\right)^2 - 34.94\left(\frac{a_0}{b}\right)^3 + 12.77\left(\frac{a_0}{b}\right)^4\right\}. \tag{15}$$

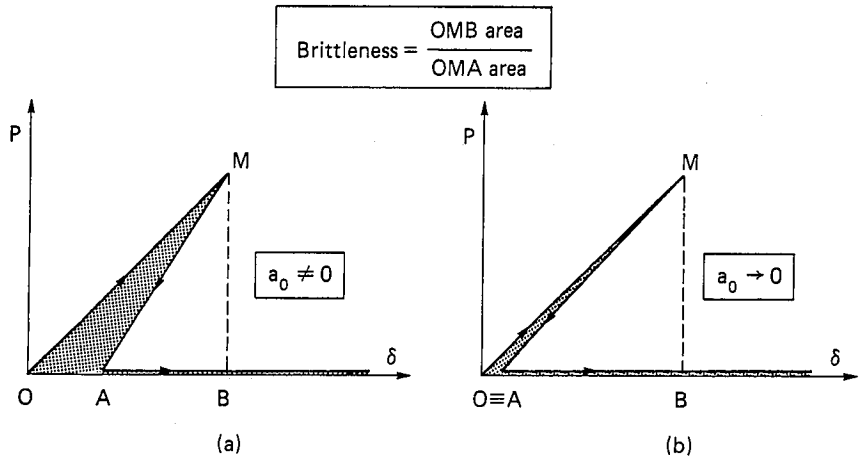

FIG. 11. Definition of structure brittleness as the ratio of elastic energy contained in the body at the bifurcation point to energy dissipated in the fracturing process. Initially cracked (a) and uncracked (b) specimen.

Relation (14) is valid also at the point of instability, and then (12) is transformed as follows:

$$\mathcal{G}_{IC}(b-a_0)t = (P_{max}\delta_{max}/2)\frac{2f^2\left(\frac{a_0}{b}\right)\left(1-\frac{a_0}{b}\right)}{\frac{1}{4}\left(\frac{\ell}{b}\right)+\frac{3}{2}g\left(\frac{a_0}{b}\right)}. \tag{16}$$

If *brittleness* is defined as the ratio of the elastic energy contained in the body at the point of instability to the energy which can be dissipated in the body (Fig. 11), it results in a function of beam slenderness and initial crack depth:

$$brittleness = \frac{\frac{1}{2}P_{max}\delta_{max}}{\mathcal{G}_{IC}(b-a_0)t} = \frac{\frac{1}{4}\left(\frac{\ell}{b}\right)+\frac{3}{2}g\left(\frac{a_0}{b}\right)}{2\left(1-\frac{a_0}{b}\right)f^2\left(\frac{a_0}{b}\right)}. \tag{17}$$

When the beam is initially uncracked, i.e. $a_0/b = 0$, the brittleness tends to infinity and the softening branch is coincident with the elastic one (Fig. 11b). On the other hand, when the initial crack length is different from zero ($a_0 \neq 0$), the brittleness tends to the value in (17) for the size-scale tending to infinity (Fig. 11a). In this case, the softening branch is always distinct from the elastic one.

When the beam is initially uncracked, the elastic energy contained in the body at the point of instability is an infinite quantity of higher rank with respect to the fracture energy, the former being proportional to $b^3(\sigma_u^2/E)$ and the latter to $b^2\mathcal{G}_{IC}$. When there is an initial crack, the two quantities are of the same rank for the size-scale b tending to infinity, their ratio being finite and provided in (17).

ACKNOWLEDGEMENTS

Some of the numerical results reported in the present paper were obtained in a joint research program between ENEL-CRIS-Milano and the University of Bologna. The Department of Public education is acknowledged for the financial support provided to the present research.

REFERENCES

BARENBLATT, G. I. 1959 *J. appl. Math. Mech.* **23,** 622.
BERRY, J. P. 1960 *J. Mech. Phys. Solids* **8,** 194.
BILBY, B. A., COTTRELL, A. H. and SWINDEN, K. H. 1963 *Proc. R. Soc.* (*London*) **A272,** 304.
BIOLZI, L., CANGIANO, S., TOGNON, G. and CARPINTERI, A. 1987 Fracture of concrete and rock, SEM-RILEM Int. Conf., to appear in *Mater. Struct.* (1989).
CARPINTERI, A. 1981 *Analytical and Experimental Fracture Mechanics*, p. 785 (edited by G. C. Sih and M. Mirabile), Sijthoff & Noordhoff, Leiden.
CARPINTERI, A. 1982 *Engng Fracture Mech.* **16,** 467.
CARPINTERI, A. 1985 *Application of Fracture Mechanics to Cementitious Composites*, p. 287 (edited by S. P. Shah), NATO-ARW, Martinus Nijhoff, Dordrecht.
DUGDALE, D. S. 1960 *J. Mech. Phys. Solids* **8,** 100.
FOOTE, R. M. L., MAI, Y. W. and COTTERELL, B. 1986 *J. Mech. Phys. Solids* **34,** 593.
GRIFFITH, A. A. 1921 *Phil. Trans. R. Soc.* **A221,** 163.
HILLERBORG, A., MODEER, M. and PETERSSON, P. E. 1976 *Cement Concrete Res.* **6,** 773.
RICE, J. R. 1968 *J. appl. Mech.* **35,** 379.
TADA, H., PARIS, P. and IRWIN, G. 1963 *The Stress Analysis of Cracks Handbook*, Vol. 2, p. 16, Del Research Corp., Hellertown, Pennsylvania.
WILLIS, J. R. 1967 *J. Mech. Phys. Solids* **15,** 151.
WNUK, M. P. 1974 *J. appl. Mech.* **41,** 234.